First simultaneous global measurements of nighttime stratospheric NO2 and NO3 observed by Global Ozone Monitoring by Occultation of Stars (GOMOS)/Envisat in 2003

Alain Hauchecorne, Jean-Loup Bertaux, Francis Dalaudier, Charles Cot, Jean-Claude Lebrun, Slimane Bekki, Marion Marchand, E. Kyrölä, J. Tamminen, Viktoria Sofieva, et al.

First simultaneous global measurements of nighttime stratospheric NO_2 and NO_3 observed by Global Ozone Monitoring by Occultation of Stars (GOMOS)/Envisat in 2003

A. Hauchecorne,[1] J.-L. Bertaux,[1] F. Dalaudier,[1] C. Cot,[1] J.-C. Lebrun,[1] S. Bekki,[1] M. Marchand,[1] E. Kyrölä,[2] J. Tamminen,[2] V. Sofieva,[2] D. Fussen,[3] F. Vanhellemont,[3] O. Fanton d'Andon,[4] G. Barrot,[4] A. Mangin,[4] B. Théodore,[4] M. Guirlet,[4] P. Snoeij,[5] R. Koopman,[6] L. Saavedra de Miguel,[6] R. Fraisse,[7] and J.-B. Renard[8]

Received 17 December 2004; revised 13 May 2005; accepted 11 July 2005; published 20 September 2005.

[1] The Global Ozone Monitoring by Occultation of Stars (GOMOS) stellar occultation instrument on board the Envisat European satellite provides global coverage of ozone and other stratospheric species with good vertical resolution and a self-calibrating method. In this paper we present the first simultaneous global distribution of stratospheric NO_2 and NO_3 from 1 year of nighttime GOMOS data in 2003. Most previous NO_2 satellite observations have been made using the solar occultation technique. They are difficult to interpret due to the fast photochemical evolution of NO_2 at sunrise and sunset. There are no published observations of NO_3 from space because this constituent is rapidly photodissociated during daytime and is not observable by solar occultation. It is shown that the NO_2 mixing ratio reaches a maximum around 40 km with values between 14 and 16 ppbv at low and middle latitudes. The global distribution of NO_2 observed by GOMOS is very similar to the NO + NO_2 Halogen Occultation Experiment climatology deduced from sunset measurements from 1999 to 2004. At high latitude a high mixing ratio is observed in the north vortex in November 2003 after a strong solar proton event and in the south vortex in July 2003. The NO_3 mixing ratio peaks at 40–45 km. NO_3 follows a semiannual variation at low latitudes with maxima at equinoxes and an annual variation at middle and high latitudes with a maximum in summer. In the upper stratosphere the mixing ratio of NO_3 is strongly correlated with temperature due to the thermal dependence of its formation rate.

Citation: Hauchecorne, A., et al. (2005), First simultaneous global measurements of nighttime stratospheric NO_2 and NO_3 observed by Global Ozone Monitoring by Occultation of Stars (GOMOS)/Envisat in 2003, *J. Geophys. Res.*, *110*, D18301, doi:10.1029/2004JD005711.

1. Introduction

[2] Odd nitrogen species play an important role in the photochemistry of stratospheric ozone. In the middle and upper stratosphere they participate in the catalytic destruction of ozone. In the lower stratosphere they form reservoir species like $ClONO_2$ which inhibit the efficiency of the catalytic destruction by halogen gases.

[3] The main source of NO_2 is the photolysis of N_2O by solar UV radiation. Other significant potential sources are the upward transport of NO_2 produced by lightning in the tropical upper troposphere and the downward transport of NO from the thermosphere or the mesosphere in the winter polar vortex.

[4] NO_2 profiles have been measured from space by several instruments. Most observations were performed using the solar occultation technique, Stratospheric Aerosol and Gas Experiment (SAGE) II [*Cunnold et al.*, 1991], Halogen Occultation Experiment (HALOE) [*Gordley et al.*, 1996], Polar Ozone and Aerosol Measurement (POAM) III [*Randall et al.*, 2002], during sunrise or sunset when the concentration is changing very quickly, which makes the interpretation very difficult. Some others were obtained from the measurement of sunlight scattering at limb during daytime, Solar Mesospheric Experiment (SME) [*Mount et al.*, 1984], Odin Spectrometer and IR Imager System

[1]Service d'Aéronomie/Institut Pierre Simon Laplace, Centre National de la Recherche Scientifique, Verrières-le-Buisson, France.
[2]Finnish Meteorological Institute, Earth Observation, Helsinki, Finland.
[3]Belgian Institute for Space Aeronomy, Brussels, Belgium.
[4]ACRI-ST, Sophia-Antipolis, France.
[5]European Space Agency/European Space Research and Technology Centre, Noordwijk, Netherlands.
[6]European Space Agency/European Space Research Institute, Frascati, Italy.
[7]European Aeronautic Defence and Space–Astrium, Toulouse, France.
[8]Laboratoire de Physique et Chimie de l'Environnement, Centre National de la Recherche Scientifique, Orleans, France.

0148-0227/05/2004JD005711

(OSIRIS) [*Sioris et al.*, 2003] and are not directly comparable with Global Ozone Monitoring by Occultation of Stars (GOMOS) due to the strong diurnal cycle of NO_2. A few nighttime observations are available for limited periods. They were obtained from the detection of the limb infrared emission by Limb Infrared Monitor of the Stratosphere (LIMS) from October 1978 to May 1979 [*Russell et al.*, 1988], Improved Stratospheric and Mesospheric Sounder (ISAMS) from September 1991 to July 1992 [*Reburn et al.*, 1996] and Cryogenic Limb Array Etalon Spectrometer (CLAES) from October 1991 to May 1993 [*Danilin et al.*, 1999]. Michelson Inteferometer for Passive Atmospheric Sounding (MIPAS) [*Fischer and Oehlaf*, 1996] on board Envisat is also providing such observations since July 2002. Local NO2 profiles are also obtained by several balloon-borne instruments including stellar and moon occultation spectrometers [*Renard et al.*, 1996, 2001], a Michelson interferometer MIPAS-Balloon (MIPAS-B) [*Friedl-Vallon et al.*, 2004]) and a Fourier transform interferometer Far Infrared Spectrometer (FIRS)-2 [*Johnson et al.*, 1995].

[5] NO_3 is a transition species for the transformation of NO_2 into the N_2O_5 reservoir during night. There are no published observations of NO_3 profiles because this species is rapidly photodissociated during daytime and is undetectable by solar occultation or limb scattering observation. SAGE III, launched in December 2001, has the capability to measure NO_3 in moon occultation mode but the results are not yet published. A few local profiles were obtained up to 40 km at mid and high latitudes by balloon-borne stellar and moon occultation instruments [*Renard et al.*, 1996, 2001].

[6] GOMOS, on board the European satellite Envisat launched 1 March 2002, is the first space instrument dedicated to the study of the atmosphere of the Earth by the technique of stellar occultation [*Bertaux et al.*, 2004]. When a star sets behind the atmosphere, its light is absorbed by atmospheric constituents. Each constituent can be identified by its absorption spectrum. The atmospheric transmission spectrum is equal to the ratio between the star spectrum absorbed by the atmosphere and the reference star spectrum outside the atmosphere. As the reference spectrum is measured at the beginning of each occultation, we can consider GOMOS as a self-calibrated instrument, independent of any radiometric calibration. With four spectrometers, the wavelength coverage from 248 nm to 942 nm allows monitoring ozone, H_2O, NO_2, NO_3, atmospheric density from Rayleigh extinction, aerosols, O_2 and temperature profiles from the upper troposphere to the mesosphere. Two additional fast photometers (1 kHz sampling rate) are used to correct star scintillation perturbations and to determine high vertical resolution temperature profiles.

[7] The main objective of the GOMOS/Envisat instrument is to build a very accurate global climatology of ozone and chemical species involved in ozone photochemistry. This climatology will be used to study the atmospheric natural variability, to test the validity of chemistry transport models and as a reference for future trend studies. GOMOS nighttime measurements are especially well adapted for this task due to their self-calibrating nature and the perfect knowledge of their altitude, a particularity of the star occultation technique. The goal of this paper is to present first simultaneous global measurements from space of nighttime NO_2 and NO_3 observed by GOMOS in 2003.

2. Data Processing

[8] Results presented here are obtained using version V6.0 of the algorithms. This version has been implemented in April 2004 for the full reprocessing of 2003 data. It is not yet fully validated, especially for NO_2 and NO_3, due to the small number of available validation data in nighttime conditions. A few profiles have been compared with those of a balloon-borne moon occultation instrument in the frame of Atmospheric Chemistry Validation (ACVE2) by *Renard et al.* [2004]. They conclude that balloon and GOMOS profiles compare reasonably well on the average although GOMOS is not able to capture fine-scale vertical structures seen in balloon profiles. Further validation is needed to improve our confidence in the quality of GOMOS data. However, this kind of exercise is limited by the difficulty to find good coincidences in time and space and we consider very useful to present a full year of GOMOS NO_2 band NO_3 measurements even if they are not fully validated. Furthermore, the internal consistency of the data gives us confidence in their quality, at least for averaged profiles for which the random error is minimized. Our results will be available for comparison with those of other satellites instruments and with the outputs of chemistry transport models on a global basis.

[9] The main characteristics of the data inversion in V6.0 are summarized below. The inversion of spectrometer data from level 1b (calibrated transmission spectra) to level 2 (vertical profiles of constituents) is made in two steps, the spectral inversion and the vertical inversion.

2.1. Spectral Inversion

[10] The goal of the spectral inversion is to determine the number of molecules along the line of sight (slant densities) of each absorber from the transmission spectrum corrected from refraction effects. In the prelaunch algorithm, a global spectral inversion was made simultaneously on all retrieved species (O_3, NO_2, NO_3, aerosols with a $1/\lambda$ extinction dependence and air density) using a Levenberg-Marquardt nonlinear least square method [*Press et al.*, 1986] to fit the measured transmission by the model transmission. More details are given by *Kyrölä et al.* [2004]. This global method was also used by *Yee et al.* [2002] for the inversion of UV and visible spectra from the Midcourse Space Experiment (MSX) satellite. It worked well for ozone at all altitudes and for minor species (NO_2 and NO_3) above 40 km. Below 40 km, spectra are affected by scintillations due to small-scale atmospheric turbulent structures and vertical line density profiles of NO_2 and NO_3 exhibited often large unrealistic fluctuations. In order to solve this problem, a differential optical absorption spectroscopy (DOAS) method was implemented in V6.0 for these two species. The DOAS principle is to determine the densities of trace gases by measuring their specific narrow band absorption structures [*Platt*, 1994]. In our case, the differential spectrum is obtained by removing a 15 nm (30 nm) moving average respectively for NO_2 (NO_3). The temperature dependence of

NO_2 and NO_3 cross sections is taken into account using ECMWF temperatures along the line of sight.

2.2. Vertical Inversion

[11] The goal of the vertical inversion is to compute local density profiles as a function of altitude from slant density profiles as a function of tangent altitude. In the prelaunch algorithm, the vertical inversion was made using an onion peeling method with a linear interpolation between layers. This method may amplify oscillations due to noisy data and scintillations, especially in the bottom of the profiles where the altitude sampling is reduced by the refraction. In order to attenuate this effect, a Tikhonov inversion technique with a second difference smoothness constraint [*Kyrölä et al.*, 1993] is applied in V6.0 with a constant vertical resolution fixed to 4 km in the case of NO_2 and for NO_3 A similar method was used by *Yee et al.* [2002]. It is worth to note that this method does not use an a priori profile.

2.3. Data Accuracy

[12] The uncertainty on local densities includes a random part due to photon counting, detector noise and chromatic scintillation effect and a systematic part due to uncertainties in the data processing parameters (cross sections, instrument spectral resolution). The random error depends on the brightness of the star in the spectral range of strongest absorption by the retrieved species (400–450 nm for NO_2 and 630–670 nm for NO_3). These two spectral bands are not too far from 550 nm used for the definition of the visual magnitude. If we consider only the 70 brightest stars (visual magnitude < 2.25), the random error of an individual profile is not larger than 20% for NO_2 between 25 and 45 km and 30% for NO_3 between 30 and 45 km and increases to 40% at 50 km and 20 km for NO_2 and 60% at 50 km and 25 km for NO_3 and higher values above and below these altitude ranges. For this study, we limit the data analysis to 20–50 km for NO_2 and 25–50 km for NO_3. Outside these altitude ranges GOMOS data have to be considered with caution. The systematic error is more difficult to estimate. Uncertainties in cross sections and on their dependence on temperature may have a significant contribution to the error budget. *Vandaele et al.* [2002] report up to 7% differences between NO_2 cross sections measured by different groups and *Orphal et al.* [2003] mention up to 10% differences for NO_3. For the present study, we use monthly mean profile in 15° latitude bands resulting from the average of 100–500 individual profiles. The random error is reduced to only a few percent (inversely proportional to the square root of the number of profiles) and the total error budget is dominated by systematic errors which are not or less reduced by the averaging process. It can be roughly estimated to 10% for NO_2 and 15% for NO_3.

3. Data Selection and Averaging

[13] One difficulty of the stellar occultation technique is the sensitivity of the data quality to star characteristics (brightness, temperature) and to viewing geometry (sun azimuth and elevation, occultation obliquity). Furthermore, for a given star, the latitude of the tangent point depends on the day of the year and the latitude coverage changes with time. In order to build three-dimensional NO_2 and NO_3 fields as homogeneous as possible, a three-step selection and averaging procedure is applied. (1) We use only the 70 brightest stars and we discard daylight observations to eliminate too noisy NO_2 and NO_3 profiles. (2) For a given star and during 1 day, the latitude of the tangent point is almost constant and the star is occulted 14 or 15 times (once per orbit) with a 25° westward longitude shift per orbit. A daily mean profile is computed as the weighted average of all available profiles amongst the 14–15 ones. Weights are inversely proportional to the squared inverse error estimates. Each daily mean profile can be considered as a zonal average at the mean latitude of the tangent point. (3) All daily mean profiles for 1 month and within a 15° latitude band are averaged taking into account their weights as indicated in step 2.

4. Results and Discussion

4.1. NO_2

[14] Partitioning of odd nitrogen family, defined as $NO + NO_2 + NO_3 + N_2O_5$, is controlled in the stratosphere by the fast photochemical equilibrium between NO and NO_2 and the slow photodissociation of N_2O_5 during daytime and the slow conversion of NO_2 into NO_3 and then into N_2O_5 during nighttime. Owing to these photochemical reactions, the NO_2 concentration is never constant. It is slowly decreasing by night and increasing by day and rapidly increasing at sunset and decreasing at sunrise. It is therefore very important to take into account the local time when comparing measurements made by different instruments. In the case of GOMOS, nighttime observations are made during the ascending path of Envisat and the local time is approximately equal to the local hour of the ascending node, 1000 LT.

[15] GOMOS provides NO_2 vertical profiles in absolute concentration as a function of geometric altitude. For photochemistry studies and comparison with other measurements and models, it is more convenient to consider mixing ratios. Figure 1 shows latitude-altitude maps of NO_2 for each month in 2003 except May where very few measurements are available due to a failure in the star pointing system. Mixing ratios have been computed using European Centre for Medium-Range Weather Forecasts (ECMWF) pressure and temperature interpolated to the time and location of GOMOS measurements. At mid and low latitudes, a maximum in the vertical profile is observed around 40 km in both hemispheres. The peak value ranges from 14 to 16 ppbv depending on the month and its latitude location varies between 20°S and 20°N with a shift toward the summer/autumn hemisphere, to the south from February to April and to the north from August to November. This value is slightly smaller than the results of *Reburn et al.* [1996] who found a 17 ppbv peak of nighttime NO_2 around 3 hPa (~40 km) in ISAMS and LIMS January data at equatorial and south tropical latitudes. At high latitude, lower values are observed in general, except when a strong descent of air enriched in NO_x ($NO + NO_2$) of mesospheric or thermospheric origin occurs inside the winter polar vortex. It is interesting to note the strong peak of NO_2 above 38 km, with up to 38 ppbv at 50 km, in the northern high latitude upper stratosphere in November. This peak has been attributed by *Seppälä et al.* [2004] to the formation of

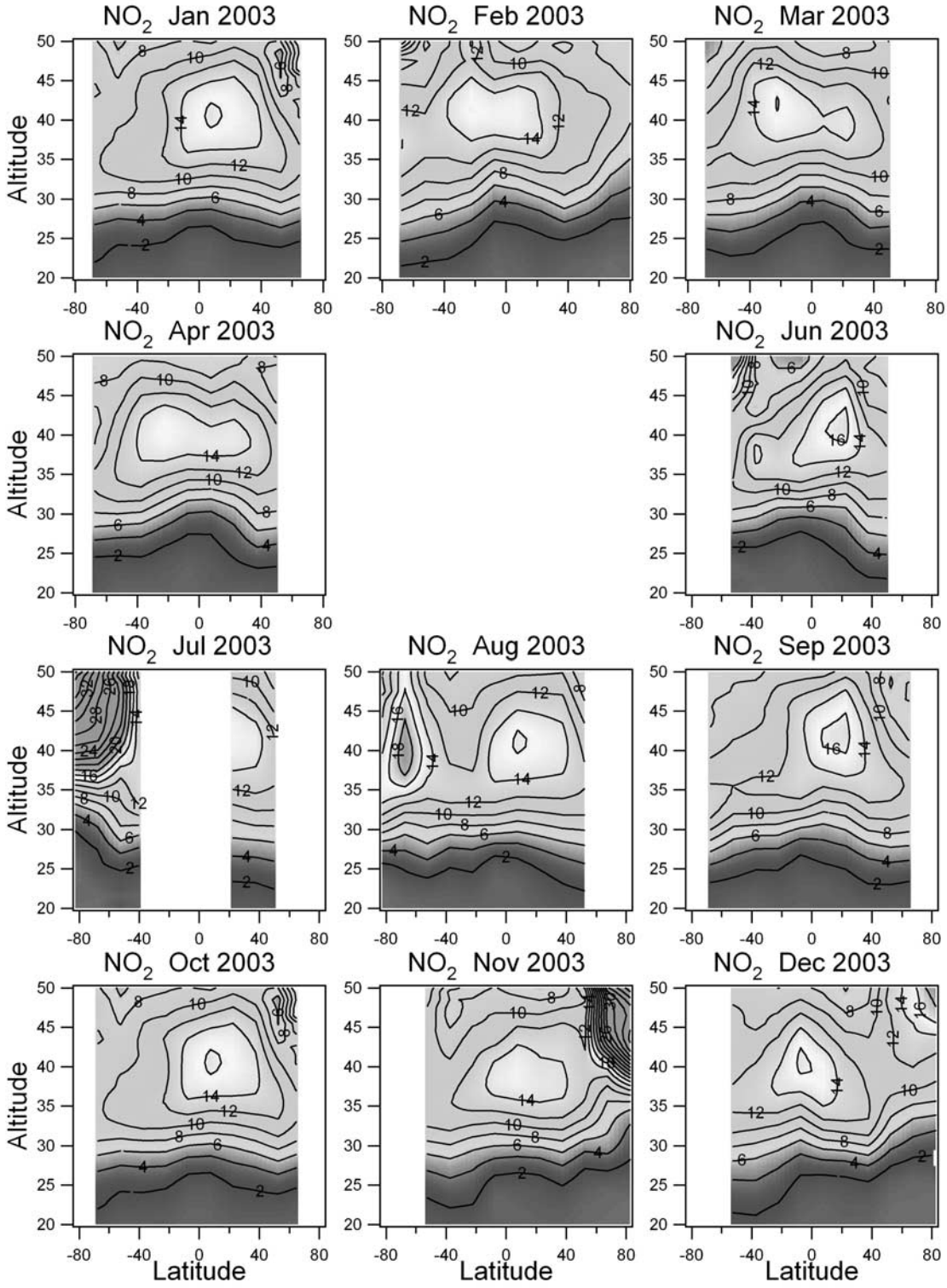

Figure 1. Latitude-altitude maps of NO_2 mixing ratio in ppbv for each month in 2003. See color version of this figure in the HTML.

a large amount of NO_x during the very intense solar proton event at the end of October 2003. Such NO_2 enhancement after strong solar proton events have been observed and simulated in the past [*Jackman et al.*, 2000, 2001; *Verronen et al.*, 2002]. A very high mixing ratio (up to 36 ppbv at 50 km) is also detected in July at southern high latitude. It is probably be due to the strong diabatic descent of mesospheric and thermospheric air with high NO_x mixing ratio in the southern winter polar vortex and a contribution of two moderate solar proton events occurring on 28–30 May and

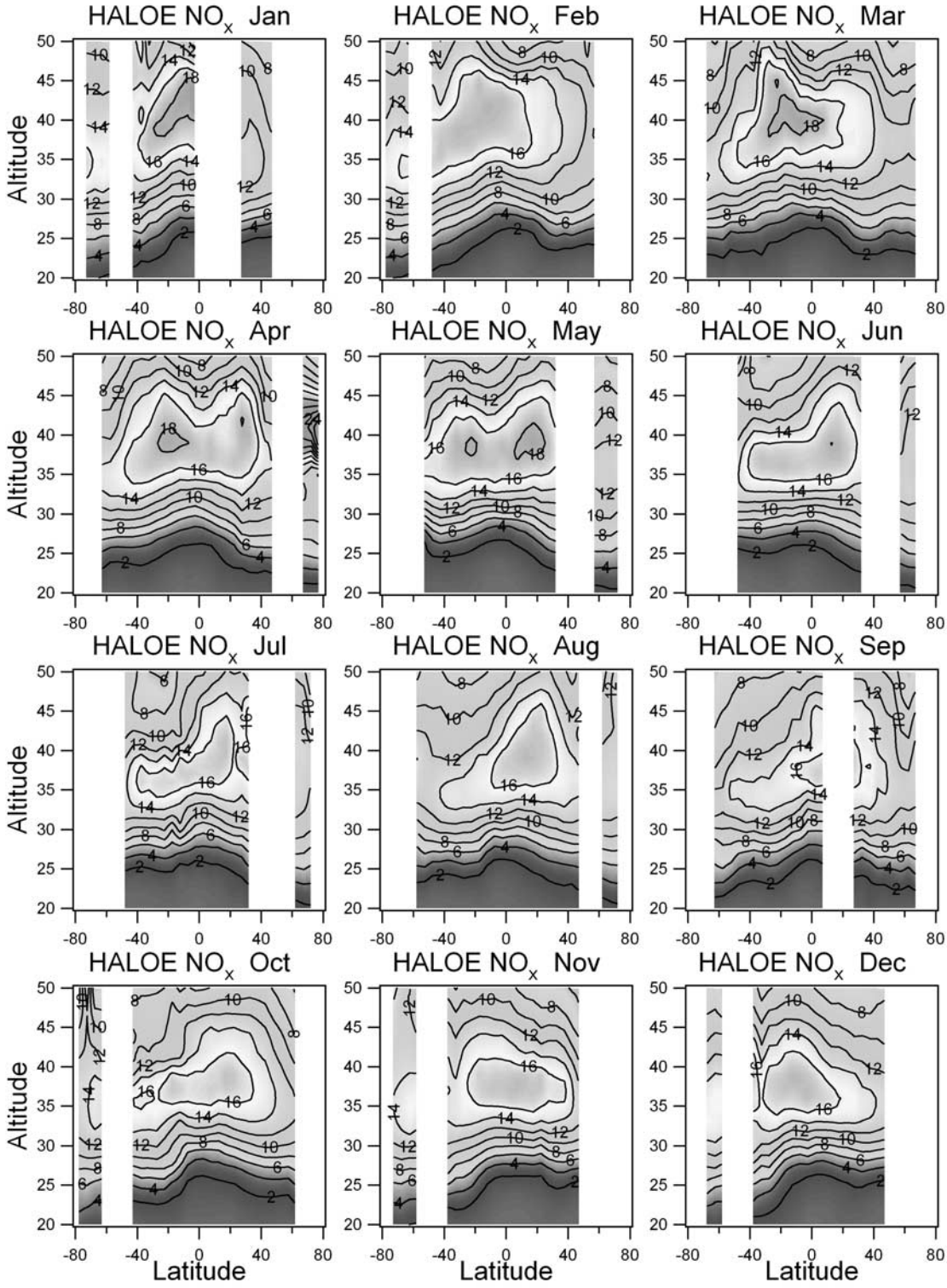

Figure 2. Latitude-altitude maps of Halogen Occultation Experiment (HALOE) NO_x (NO + NO_2) mixing ratio at sunset in ppbv for each month (average from 1999 to 2004). See color version of this figure in the HTML.

18 June is not excluded. Further studies are needed to analyze and interpret these observations in cooperation with modelers.

[16] Our understanding of the global climatology of NO and NO_2 is largely based today on solar occultation instruments. It is then very interesting to compare our results with those of a well validated solar instrument. A reasonable comparison can be made with HALOE sunset NO + NO_2 data. By sunset, most of the N_2O_5 reservoir has been converted to NO and NO_2. Shortly after sunset the NO is

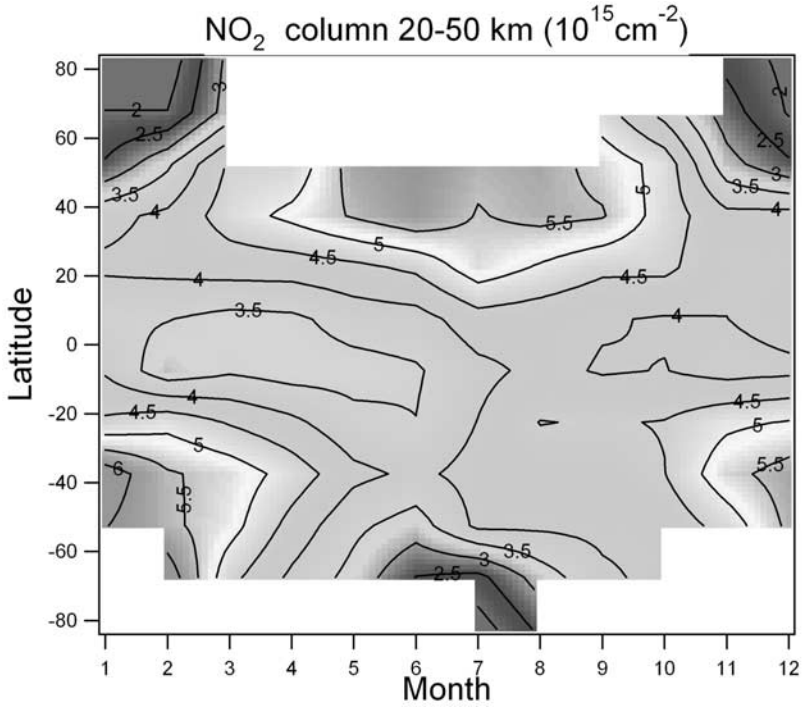

Figure 3. Time-latitude cross section of NO_2 stratospheric column (20–50 km) in 10^{15} cm^{-2} in 2003. See color version of this figure in the HTML.

converted to NO_2, which then converts slowly to N_2O_5 during the night. Thus the sum NO + NO_2 at sunset is a reasonable proxy for the NO_2 that GOMOS measures at 1000 LT. A NO_x climatology, built from HALOE sunset data from 1999 to 2004, extracted from the Web site http://haloedata.larc.nasa.gov/home/index.php, is presented in Figure 2. A direct comparison with HALOE data in 2003 was not possible due to too many data gaps. At low and mid latitudes, peak mixing ratios range from 16 to 18 ppmv, about 2 ppmv higher than in GOMOS NO_2. This may be explained by the slow conversion of NO_2 into N_2O_5 between sunset and 1000 LT. It is very interesting to note that the location and the shape of the maximum presents many similarities between both data sets, for instance the shift of the maximum toward the summer/autumn hemisphere and the double peak structure from March to June. At high latitude, high values observed by GOMOS are not visible in HALOE data. This may be due to the fact that they are caused by specific phenomena occurring only in 2003 like the October 2003 solar proton event or to the limited HALOE coverage at high latitudes in winter. Several space-borne instruments, as well as many ground-based UV-visible spectrometers, provide daily total columns of NO_2. For future comparison with such observations and for geophysical studies, GOMOS NO_2 stratospheric columns are computed by integration of profile concentrations between 20 and 50 km. This altitude range is chosen to integrate most of stratospheric NO_2 and to avoid too noisy data at low altitude. Contrary to mixing ratios that are maximum around 40 km, altitudes lower than 35 km contribute to 70 to 80% to the column. At midlatitude, NO_2 columns (Figure 3) follow a strong annual cycle with a maximum > 6.0 10^{15} cm^{-2} in summer and a minimum < 3 10^{15} cm^{-2} in winter. Low values are observed at high latitude in winter (<2.0 10^{15} cm^{-2}) in relation to the conversion of NO_2 into N_2O_5 in the polar night and to the heterogeneous conversion of NO_x into HNO_3 [*Goutail et al.*, 1994] in presence of polar stratospheric clouds. At low latitude, a weak annual variation is observed, in phase in the two hemispheres, with a minimum from February to April and a maximum from August to January.

4.2. NO_3

[17] The nighttime NO_3 concentration is controlled by the three reactions [*Brasseur and Solomon*, 1986]

$$\text{(R1)} \qquad NO_2 + O_3 \rightarrow NO_3 + O_2,$$

$$\text{(R2)} \qquad NO_2 + NO_3 + M \rightarrow N_2O_5 + M,$$

$$\text{(R3)} \qquad N_2O_5 \rightarrow NO_2 + NO_3.$$

Below 40 km, the thermal decomposition (reaction (3)) can be neglected and reaction (2) is fast enough for NO_3 to reach steady state equilibrium in less than 1 hour after sunset typically. NO_3 concentration is proportional to O_3 and is positively correlated with temperature through reaction (1). As pointed out by *Renard et al.* [2005], this strong dependence on temperature may induce biases in individual vertical NO_3 profiles in the presence of local temperature fluctuations. However, monthly mean profiles will not be too much affected. Above 40 km, the thermal decomposition is a significant source of NO_2 after sunset and reaction (2) is much slower. As a result, NO_3 is no more

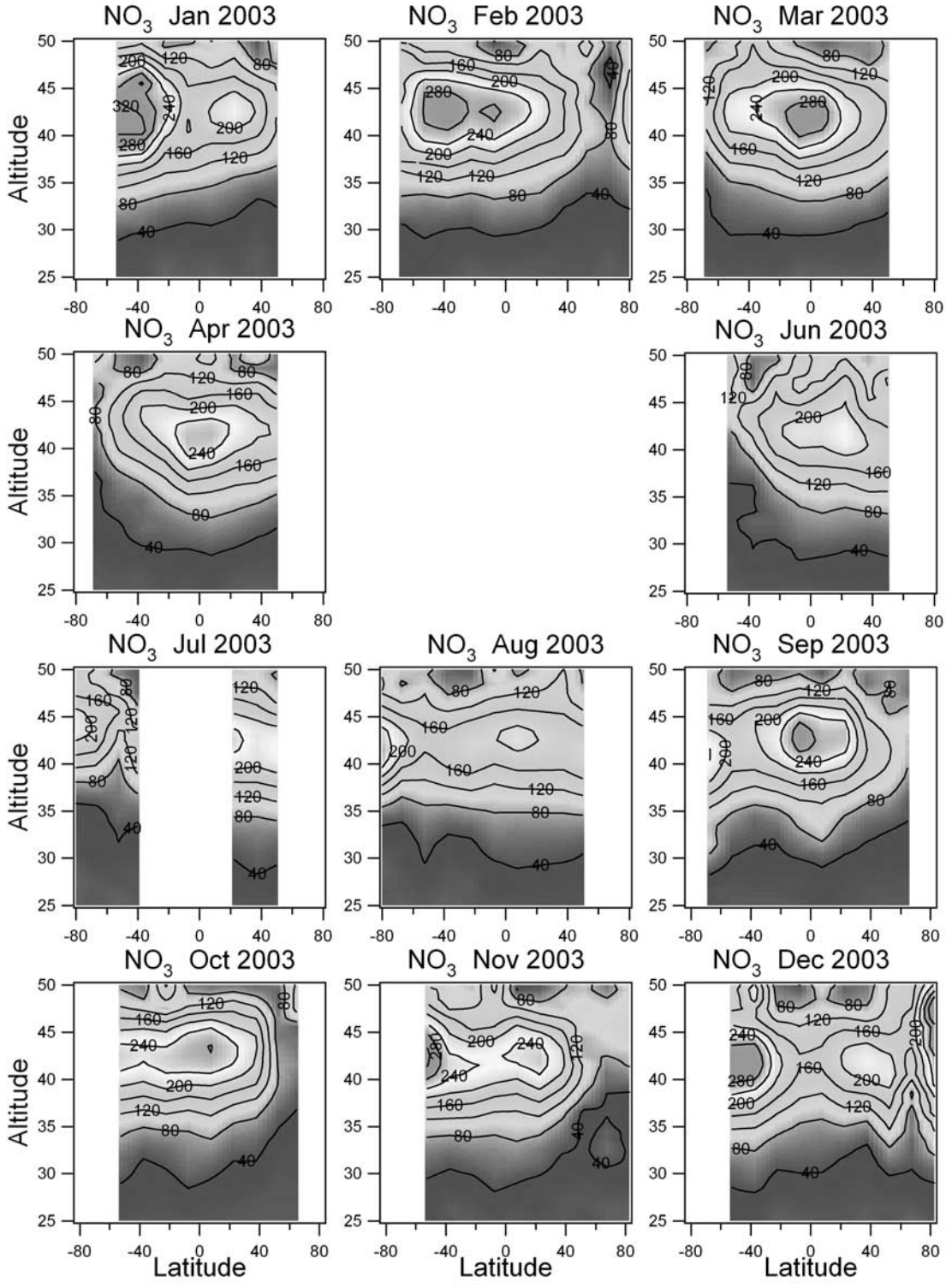

Figure 4. Latitude-altitude cross section of NO_3 mixing ratio in pptv for each month in 2003. See color version of this figure in the HTML.

at equilibrium at the time of GOMOS observations [*Marchand et al.*, 2004] and is dependent on both NO_2 and O_3 concentrations.

[18] The maximum mixing ratio is reached between 41 and 43 km (Figure 4). At mid latitude, values are higher in the summer hemisphere than in the winter one (up to 320 pptv at southern midlatitude in January). At low latitudes, the variation is more semiannual with maxima in February–March and September and minima in December–January and June–August. High values are observed at northern high latitudes in the north in December at the time of a sudden stratospheric warming.

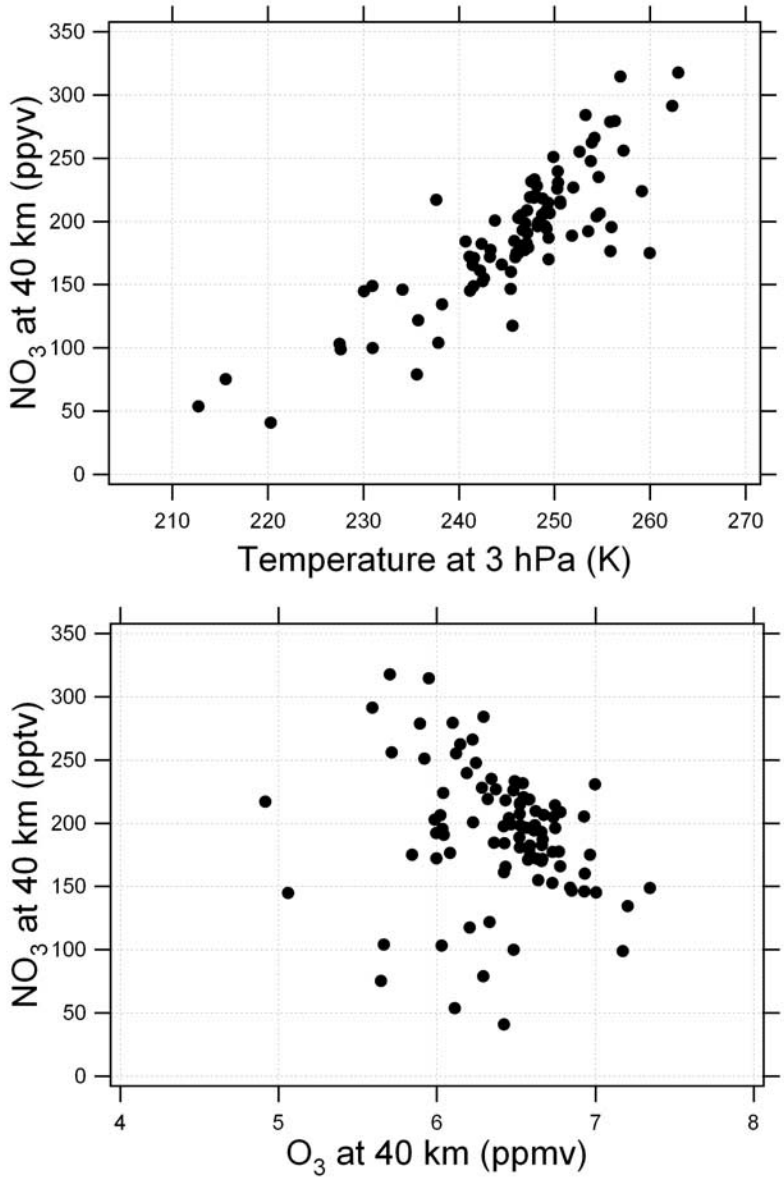

Figure 5. (top) NO_3 mixing ratio at 40 km versus European Centre for Medium-Range Weather Forecasts (ECMWF) temperature at 3 hPa (~40 km). (bottom) NO_3 mixing ratio at 40 km versus O_3 mixing ratio at 40 km for all monthly averaged latitude binned data between 60°S and 60°N.

All these results suggest that NO_3 evolution is linked with upper stratospheric temperature. Warmer temperatures increase the production rate of NO_3 through the temperature dependence of reaction (1). To test this hypothesis, the monthly average of ECMWF temperature at 3 hPa (~40 km) has been computed for each 15° latitude band between 60°S and 60°N and correlated with the corresponding NO_3 mixing ratio (Figure 5 (top)). There is a very clear correlation between both parameters. On the contrary, NO_3 at 40 km does not seem to be correlated with O_3 at 40 km (Figure 5 (bottom)) which is almost constant at this altitude. Another mechanism may contribute to high NO_3 values at northern high latitudes in December. *Orsolini et al.* [2005] attribute the large HNO_3 increase observed by MIPAS at this time to the strong increase of NO_y in the Arctic upper stratosphere after the October 2003 solar proton event. This increase will enhance the production of NO_3 through reaction (1). Further studies are needed to evaluate the contribution of the two proposed mechanisms.

[19] NO_3 stratospheric columns have been computed by integration of concentration profiles in the limited altitude range 25–50 km in order to avoid too noisy data in the lower stratosphere. The seasonal evolution of the column as a function of latitude is quite similar to the evolution of the peak mixing ratio (Figure 6). A strong annual variation is observed at mid and high latitudes with a summer maximum higher in the south than in the north. In the north, the effect of the December polar stratospheric warming is also visible in the column. At low latitude, the evolution is more

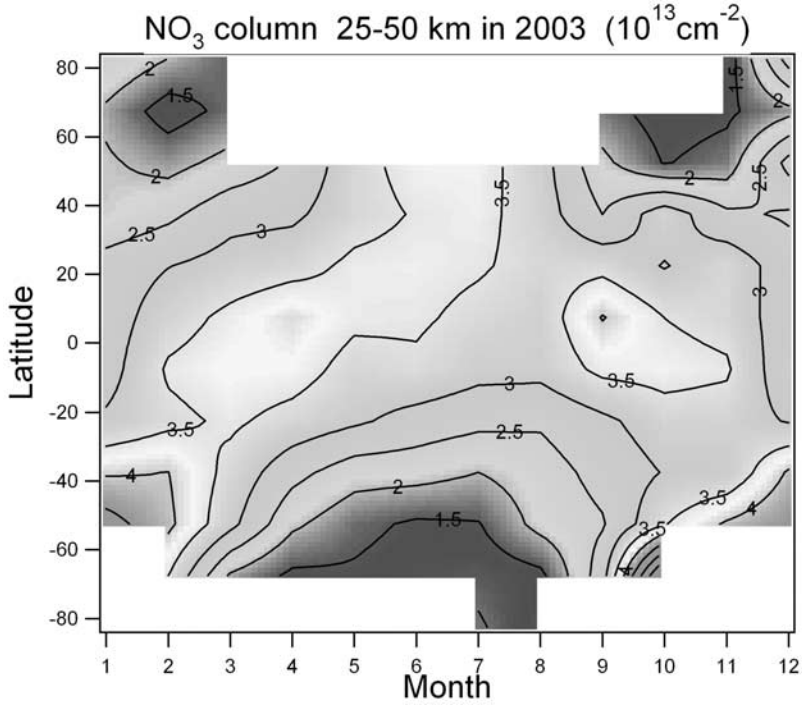

Figure 6. Time-latitude cross section of NO_3 stratospheric column (25–50 km) in 10^{13} cm^{-2} in 2003. See color version of this figure in the HTML.

semiannual with maxima in March–April and September–October and minima in December–January and June–July.

5. Conclusion

[20] GOMOS provides for the first time simultaneous global measurements of stratospheric NO_2 and NO_3 during night. The full reprocessing of 2003 data allowed us to follow the seasonal evolution of these two species as a function of latitude. The main results of this study are summarized below.

[21] 1. For NO_2, at low and mid latitudes, the mixing ratio reaches a maximum around 40 km with 14 to 16 ppbv. These values are about 2 ppbv lower than the sum NO + NO_2 measured by HALOE at sunset. The difference can be explained by the slow conversion of NO_2 into N_2O_5 between sunset and 10pm local time. The location of the maximum is shifted toward the summer/autumn hemisphere in both data sets. A high mixing ratio is also observed in upper stratosphere in November in the north polar vortex after a strong solar proton event and in July in the south vortex when air enriched in NO_x descends from the mesosphere and the thermosphere. At low latitude, NO_2 stratospheric columns follow an annual variation in phase in the two hemispheres with a minimum from February to April and a maximum from August to January. At middle and high latitudes, the annual cycle of NO_2 columns is of large amplitude with a maximum in summer.

[22] 2. For NO_3, the mixing ratio peaks at 40–45 km. At low latitude, a semiannual variation is observed in NO_3 peak concentration and stratospheric column with a maximum at equinoxes. At middle and high latitudes, the variation of NO_3 is annual with a maximum in summer. The NO_3 mixing ratio in the upper stratosphere is strongly correlated with temperature through the thermal dependence of reaction $NO_2 + O_3 \rightarrow NO_3 + O_2$.

[23] These results are still preliminary and more validation studies will be done in the future but they provide a first full global view of two important odd nitrogen species. They are available for model studies to test photochemistry on NO_x in the stratosphere and for comparison with other satellite, in situ and ground-based observations. One of the main advantages of GOMOS is a better geographical coverage than solar occultation instruments upon which so much of our understanding today is based.

[24] **Acknowledgments.** Envisat is a European Space Agency (ESA) mission. We are especially grateful for the tremendous work of Guido Levrini and Jacques Louet for the success of the mission.

References

Bertaux, J.-L., et al. (2004), First results on GOMOS/ENVISAT, *Adv. Space Res.*, *33*, 1029–1035.

Brasseur, G., and S. Solomon (1986), *Aeronomy of the Middle Atmosphere*, D. Reidel, Norwell, Mass.

Cunnold, D. M., et al. (1991), Validation of SAGE II NO_2 measurements, *J. Geophys. Res.*, *96*, 12,913–12,925.

Danilin, M. Y., et al. (1999), Nitrogen species in the post-Pinatubo stratosphere: Model analysis utilizing UARS measurements, *J. Geophys. Res.*, *104*, 8247–8262.

Fischer, H., and H. Oehlaf (1996), Remote sensing of vertical profiles of atmospheric trace constituents with MIPAS limb-emission spectrometers, *Appl. Opt.*, *35*, 2796–2797.

Friedl-Vallon, F., G. Maucher, A. Kleinert, A. Lengel, C. Keim, H. Oehlaf, H. Fischer, M. Seefeldner, and O. Trieschmann (2004), Design and characterization of the balloon-borne Michelson Interferometer for Passive Atmospheric Sounding, *Appl. Opt.*, *43*, 3335–3355.

Gordley, L. L., et al. (1996), Validation of nitric oxide and nitrogen dioxide measurements made by Halogen Occultation Experiment for UARS platform, *J. Geophys. Res.*, *101*, 10,241–10,266.

Goutail, F., J.-P. Pommereau, A. Sarkissian, E. Kyro, and V. Dorokhov (1994), Total nitrogen dioxide at the Arctic polar circle since 1990, *Geophys. Res. Lett.*, *21*, 1371–1374.

Jackman, C. H., E. L. Fleming, and F. M. Vitt (2000), Influence of extremely large solar proton events in a changing stratosphere, *J. Geophys. Res.*, *105*, 11,659–11,670.

Jackman, C. H., R. D. McPeters, G. J. Labow, E. L. Fleming, C. J. Praderas, and J. M. Russell (2001), Northern Hemisphere atmospheric effects due to the July 2000 solar proton event, *Geophys. Res. Lett.*, *28*, 2883–2886.

Johnson, D. G., K. W. Jucks, W. A. Traub, and K. V. Chance (1995), The Smithsonian Far-Infrared Spectrometer and data reduction system, *J. Geophys. Res.*, *100*, 3091–3106.

Kyrölä, E., E. Sihvola, Y. Kotivuori, M. Tikka, and T. Tuomi (1993), Inverse theory for occultation measurements: 1. Spectral inversion, *J. Geophys. Res.*, *98*, 7367–7381.

Kyrölä, E., et al. (2004), GOMOS on Envisat: An overview, *Adv. Space Res.*, *33*, 1020–1028.

Marchand, M., S. Bekki, A. Hauchecorne, and J.-L. Bertaux (2004), Validation of the self-consistency of GOMOS NO_3, NO_2 and O_3 using chemical datam assimilation, *Geophys. Res. Lett.*, *31*, L10107, doi:10.1029/2004GL019631.

Mount, G. H., D. W. Rusch, J. F. Noxon, J. M. Zawodny, and C. A. Barth (1984), Measurements of stratospheric NO_2 from solar mesosphere explorer satellite: 1. An overview of the results, *J. Geophys. Res.*, *89*, 1327–1340.

Orphal, J., C. E. Fellows, and P.-M. Flaud (2003), The visible absorption spectrum of NO_3 measured by high-resolution Fourier transform spectroscopy, *J. Geophys. Res.*, *108*(D3), 4077, doi:10.1029/2002JD002489.

Orsolini, Y. J., G. L. Manney, M. L. Santey, and C. E. Randall (2005), An upper stratospheric layer of enhanced HNO_3 following exceptional solar storms, *Geophys. Res. Lett.*, *32*, L12S01, doi:10.1029/2004GL021588.

Platt, U. (1994), Differential optical absorption spectroscopy (DOAS), *Chem. Anal. Ser.*, *127*, 27–83.

Press, W. H., B. P. Flannery, S. A. Teulosky, and W. T. Vetterling (1986), *Numerical Recipes: The Art of Scientific Computing*, Cambridge Univ. Press, New York.

Randall, C. E., et al. (2002), Validation of POAM III NO_2 measurements, *J. Geophys. Res.*, *107*(D20), 4432, doi:10.1029/2001JD001520.

Reburn, W. J., J. J. Remedios, P. E. Morris, C. D. Rodgers, F. W. Taylor, B. J. Kerridge, R. J. Knight, J. Ballard, J. B. Kumer, and S. T. Massie (1996), Validation of NO_2 measurements from the ISAMS, *J. Geophys. Res.*, *101*, 9873–9895.

Renard, J.-B., M. Pirre, C. Robert, G. Moreau, D. Huguenin, and J. M. Russell (1996), Nocturnal vertical distribution of stratospheric O_3, NO_2 and NO_3 from balloon measurements, *J. Geophys. Res.*, *101*, 28,793–28,804.

Renard, J.-B., F. G. Taupin, E. D. Rivière, M. Pirre, N. Huret, G. Berthet, C. Robert, and M. Chartier (2001), Measurement and simulation of stratospheric NO_3 at mid and high latitudes in the Northern Hemisphere, *J. Geophys. Res.*, *106*, 32,387–32,399.

Renard, J.-B., et al. (2004), Validation of GOMOS vertical profiles using balloon-borne instruments and satellite data, in *Proceedings of the Second Workshop on the Atmospheric Chemistry Validation of ENVISAT (ACVE-2), ESA-ESRIN, Frascati, Italy, 3–7 May 2004*, pp. 60.1–60.7, Eur. Space Agency, Noordwijk, Netherlands.

Renard, J.-B., et al. (2005), NO_3 vertical profile measurements from remote sensing balloon-borne spectrometers and comparison with model calculations, *J. Atmos. Chem.*, *51*, 65–78.

Russell, J., J. Gille, E. Remsberg, L. Gordley, P. Bailey, S. Drayson, H. Fischer, A. Girard, J. Harries, and W. Evans (1988), Validation of nitrogen dioxide results measured by the Limb Infrared Monitor of the Stratosphere (LIMS) experiment on Nimbus 7, *J. Geophys. Res.*, *93*, 1718–1736.

Seppälä, A., P. T. Veronen, E. Kyrölä, S. Hassinen, L. Backman, A. Hauchecorne, J.-L. Bertaux, and D. Fussen (2004), Solar proton events of October–November 2003: Ozone depletion in the Northern Hemisphere polar winter as seen by GOMOS/Envisat, *Geophys. Res. Lett.*, *31*, L19107, doi:10.1029/2004GL021042.

Sioris, C. E., et al. (2003), Stratospheric profiles of nitrogen dioxide observed by Optical Spectrograph and Infrared Imager System on the Odin satellite, *J. Geophys. Res.*, *108*(D7), 4215, doi:10.1029/2002JD002672.

Vandaele, A. C., C. Hermans, S. Fally, M. Carleer, R. Colin, M.-F. Mérienne, A. Jenouvrier, and B. Coquart (2002), High-resolution Fourier transform measurement of the NO_2 visible and near-infrared absorption cross sections: Temperature and pressure effects, *J. Geophys. Res.*, *107*(D18), 4348, doi:10.1029/2001JD000971.

Verronen, P. T., E. Turunen, T. Ulich, and E. Kyrölä (2002), Modelling the effects of the October 1989 solar proton event on mesospheric odd nitrogen using a detailed ion and neutral chemistry model, *Ann. Geohys.*, *20*, 1967–1976.

Yee, J.-H., et al. (2002), Atmospheric remote sensing using a combined extinctive and refractive stellar occultation technique: 1. Overview and proof-of-concept observations, *J. Geophys. Res.*, *107*(D14), 4213, doi:10.1029/2001JD000794.

G. Barrot, O. Fanton d'Andon, M. Guirlet, A. Mangin, and B. Théodore, ACRI-ST, 260 rue du Pin Montard, BP 234, F-06904 Sophia-Antipolis, France.

S. Bekki, J.-L. Bertaux, C. Cot, F. Dalaudier, A. Hauchecorne, J.-C. Lebrun, and M. Marchand, Service d'Aéronomie/Institut Pierre Simon Laplace, Centre National de la Recherche Scientifique, B.P. 3, Reduit de Verrieres, F-91371 Verrières-le-Buisson, France. (alain.hauchecorne@aerov.jussieu.fr)

R. Fraisse, European Aeronautic Defence and Space–Astrium, F-31400 Toulouse, France.

D. Fussen and F. Vanhellemont, Belgian Institute for Space Aeronomy, 3, avenue Circulaire, B-1180 Brussels, Belgium.

R. Koopman and L. Saavedra de Miguel, European Space Agency/European Space Research Institute, Via Galileo Galilei, Casella Postale 64, I-00044 Frascati, Italy.

E. Kyrölä, V. Sofieva, and J. Tamminen, Finnish Meteorological Institute, Earth Observation, P.O. Box 503, FIN-00101 Helsinki, Finland.

J.-B. Renard, Laboratoire de Physique et Chimie de l'Environnement, Centre National de la Recherche Scientifique, 3A Avenue de la Recherche Scientifique, F-45071 Orleans, Cedex 2, France.

P. Snoeij, European Space Agency/European Space Research and Technology Centre, Keplerlaan 1, Postbus 299, Noordwijk, 2200 AG, Netherlands.